An Effective Couple Method for Reliability-Based Multi-Objective Optimization of Truss Structures with Static and Dynamic Constraints

Vo-Duy, T.; Duong-Gia, D.; Ho-Huu, V.; Nguyen-Thoi, T.

DOI
10.1142/S0219876219500166

Publication date
2019

Document Version
Accepted author manuscript

Published in
International Journal of Computational Methods

International Journal of Computational Methods

AN EFFECTIVE COUPLE METHOD FOR RELIABILITY-BASED MULTI-OBJECTIVE OPTIMIZATION OF TRUSS STRUCTURES WITH STATIC AND DYNAMIC CONSTRAINTS

T. Vo-Duy[1,2,††], D. Duong-Gia[1,†], V. Ho-Huu[3,#], T. Nguyen-Thoi[1,2,*]

[1] *Division of Computational Mathematics and Engineering, Institute for Computational Science, Ton Duc Thang University, Ho Chi Minh City, Viet Nam*

[2] *Faculty of Civil Engineering, Ton Duc Thang University, Ho Chi Minh City, Viet Nam*

[3] *Faculty of Aerospace Engineering, Delft University of Technology, Delft, The Netherlands*

[††]voduytrung@tdtu.edu.vn, [†]duongdungue@gmail.com, [#]v.hohuu@tudelft.nl, [*]nguyenthoitrung@tdtu.edu.vn

Received (Day Month Year)
Revised (Day Month Year)

This paper proposes an effective couple method for solving reliability-based multi-objective optimization problems of truss structures with static and dynamic constraints. The proposed coupling method integrates a single loop deterministic method (SLDM) into the non-dominated sorting genetic algorithm II (NSGA-II) algorithm to give the called SLDM-NSGA-II. Thanks to the advantage of SLDM, the probabilistic constraints are treated as approximating deterministic constraints. And therefore the reliability-based multi-objective optimization problems can be transformed into the deterministic multi-objective optimization problems of which the computational cost is reduced significantly. In these reliability-based multi-objective optimization problems, the conflicting objective functions are to minimize the weight and minimize the displacements of the truss. The design variables are cross-section areas of the bars and contrainsts include static and dynamic constraints. For reliability analysis, the effect of uncertainty of parameters such as force, added mass in the nodes, material properties and cross-section areas of the bars are taken into account. The effectiveness and reliability of the proposed method are demonstrated through three benchmark-type truss structures including a 10-bar planar truss, a 72-bar spatial truss and a 200-bar planar truss. Moreover, the influence of parameters on the reliability-based Pareto optimal fronts is also carried out.

Keywords: Multi-objective optimization, reliability-based multi-objective optimization, non-dominated sorting genetic algorithm II (NSGA-II), single-loop algorithm, uncertainty, static and dynamic constraints.

1. Introduction

Truss is one of the important structures in civil engineering and has a wide range of applications such as roofs, transmission towers, bridge supporters, etc. Because of its significant role, the optimization of truss structures has drawn much attention from engineers and scientists [Ho-Huu *et al*. (2016)]. To ensure the truss structures to work effectively as well as satisfy the economical requirements, the formulation of the multi-objective optimization problem for truss structures and the development of robust methods for solving the multi-objective optimization problems need to be developed.

* Corresponding author.

Over the past few decades, various studies have been done for multi-objective optimization of truss structures. For example, Coello and Christiansen (2000) proposed a new Genetic algorithm (GA)-based multi-objective optimization algorithm for truss structures. In this study, three objective functions were considered simultaneously including the minimum weight, the maximum displacement and the maximum stress; and the cross-sectional areas of elements are considered as the design variables. Luh and Chueh (2004) developed an immune algorithm for multi-objective optimization of truss structures. In this study, the multi-objective function is to minimize the volume of the structure and the vertical displacement at nodes simultaneously. The cross-sectional areas of elements are considered as design variables, and the constraints are the limit principal stresses in elements. Kelesoglu (2007) presented a genetic algorithm for solving fuzzy multi-objective optimization of space truss. In this study, the objective functions include the minimum weight and minimum displacement, and the constraints are related to the volume of construction weight, displacement, geometrical properties, cross-sectional areas, member degrees, and upper and lower limit values of the stress elements. Richardson *et al*. (2012) studied single and multi-objective topology optimization of truss-like structures using genetic algorithms. The conflicting objectives of this problem are the mass and the first natural frequency of the structure, and the constraints include the stress constraint on the members, the buckling of the members and the deflection constraint. Recently, Kaveh (2017) presented a literature review of multi-objective optimization that uses the main concepts of charged system search algorithm. As it can be seen from the above-mentioned studies, the constraints in multi-objective optimization problems were mostly focused on static constraints such as displacement and stress of structures. Nevertheless, the dynamic constraints such as frequency and buckling load factor are still somewhat limited [Gomes (2011)].

On the other hand, the optimal configuration of truss structures is highly sensitive to the random design variables (e.g. members' cross-sectional areas) or random parameters (e.g. applied loads, material modulus of elasticity). Any change of these random factors may significantly affect the performance and safety of the structures [Ho-Huu *et al.* (2016)]. Therefore, it is really necessary to consider the influence of uncertain factors during the optimization designing process which belongs to the group of the Reliability Based Design Optimization (RBDO) problems. Typically, there are three main approaches to solve RBDO including Double Loop Method (DLM), Decouple Double Loop Method (DDLM), and Single Loop deterministic method (SLDM) [Li *et al.* (2013)]. Recently, some methods that are capable of effectively handling non-probabilistic random variables, e.g., uncertain-but-bounded variables, have also been developed [Hao *et al*. (2017); Meng and Zhou (2018)]. Also, some improvements on reliability assessment methods and their combination with the above approaches have been studied [Meng *et al*. (2015), (2017)]. However, to deal with the probabilistic random variables, among these methods, the SLDM is identified as one of the most effective algorithms due to, the good potential balance between computational cost and accuracy of the optimal solutions [Shan and Wang (2008)]. The development of SLDM for single objective optimization has been conducted by many researchers as shown in

references [Jalalpour *et al*. (2013); Jeong and Park (2017); Li *et al*. (2013); Liang *et al*. (2007); Lim and Lee (2016); Mansour and Olsson (2016); Zhang (2016)]. However, the extension of the SLDM for multi-objective optimization is still very limited, especially, for truss structures.

Based on the above-mentioned research gaps, the present study is conducted to propose an effective couple method for solving the reliability-based multi-objective optimization problems of truss structures with both static and dynamic constraints. In this method, the single Loop deterministic method (SLDM) is first employed to transform a reliability-based multi-objective optimization problem to a deterministic multi-objective optimization problem. Then, a nondominated sorting genetic algorithm II (NSGA-II) [Deb *et al*. (2002)] is used to determine the Pareto-optimal solutions. The coupling method is hence called the SLDM-NSGA-II. The effectiveness and reliability of the proposed method are demonstrated through three numerical examples: 10-bar, 72-bar and 200-bar trusses. The conflicting objective functions include minimization of the weight and minimization of the displacement of truss structures, and the design variables are the cross-section areas of bars. The constraints include node displacements, element's stresses and natural frequencies. The material properties, the force, the added mass in the nodes and the cross-sectional area of each bar are considered as random variables. Some analyses are performed to investigate the effect of parameters such as reliability index, limited allowable and frequency constraint on the Pareto-optimal solutions.

The remainder of the paper is organized as follows. Section 2 briefly introduces the Single Loop Deterministic method. Section 3 briefly presents the NSGA-II algorithm. Section 4 presents the proposed couple method which integrates the single-loop deterministic method (SLDM) into the NSGA-II algorithm. Section 5 introduces the formulation of the reliability-based multi-objective optimization problem for truss structures. Section 6 examines some numerical examples, and Section 7 with draws some conclusions.

2. Single Loop Deterministic Method - Reliability Based Optimization

A typical RBDO problem is formulated as [Shan and Wang (2008)]

$$\begin{aligned} &\text{find} && \mathbf{d},\boldsymbol{\mu}_{\mathbf{x}},\boldsymbol{\mu}_{\mathbf{p}} \\ &\min && f(\mathbf{d},\boldsymbol{\mu}_{\mathbf{x}},\boldsymbol{\mu}_{\mathbf{p}}) \\ &\text{s.t.} && \mathrm{P}\left[g_i(\mathbf{d},\mathbf{x},\mathbf{p})\le 0\right]\ge r_i,\ i=1,2,...,nc \\ & && \mathbf{d}^{\text{low}}\le\mathbf{d}\le\mathbf{d}^{\text{up}},\quad \boldsymbol{\mu}_{\mathbf{x}}^{\text{low}}\le\boldsymbol{\mu}_{\mathbf{x}}\le\boldsymbol{\mu}_{\mathbf{x}}^{\text{up}} \end{aligned} \tag{1}$$

where $\mathbf{d}\in\mathbb{R}^k$ is the vector of deterministic design variables; $\mathbf{x}\in\mathbb{R}^k$ is the vector of random design variables; $\mathbf{p}\in\mathbb{R}^q$ is the vector of random parameters; $\boldsymbol{\mu}_{\mathbf{x}}$ and $\boldsymbol{\mu}_{\mathbf{p}}$ are the mean vectors of $\mathbf{x}$ and $\mathbf{p}$, respectively; r_i denotes the design reliability (or desired reliability/probability) satisfying the ith constraint. Superscripts ''low'' and ''up'' denote the minimum and maximum allowable limits, respectively.

It is known that the RBDO process is a good way to obtain a safe design with a low cost for structures under the influence of uncertainties. Nevertheless, the computational cost for solving the RBDO problem is very expensive, which becomes the main limitation for structural applications in reality. As an effort to reduce the computational burden of solving the RBDO problems, Li *et al*. (2013) proposed a procedure called the single-loop deterministic method (SLDM) that can solve the RBDO problems at a low computational cost. The method includes two steps: firstly the probabilistic constraints are converted into approximating deterministic constraints and secondly the deterministic optimization problem is established and solved. The key points of the SLDM are presented in the following sections. For more details of the method, the interested readers are encouraged to refer to the reference [Li *et al*. (2013)].

2.1. *Establishing approximating deterministic feasible regions*

In the SLDM, the probabilistic feasible region is transformed to the approximating deterministic feasible region by moving the probabilistic constraint boundary (denoted as a limit state function g_i) into the feasible design region at least a distance β_i as shown Figure 1. The notations in the figure are defined as follows: the pink curve represents the limit-state function g_i; The blue curve is the boundary of the transformed deterministic constraint $\tilde{g}_i$; The dotted area is the deterministic feasible region; $\boldsymbol{\theta} = [\mathbf{x}, \mathbf{p}]^{\mathrm{T}}$ is the vector that combines both random variables and random parameters; $\boldsymbol{\mu}_{\boldsymbol{\theta}} = [\boldsymbol{\mu}_{\mathbf{x}}, \boldsymbol{\mu}_{\mathbf{p}}]^{\mathrm{T}}$ is the mean of $\boldsymbol{\theta}$; and $\beta_i = \Phi^{-1}(r_i)$ where Φ is the normal standard distribution.

The transformation ensures that the smallest distance between any point on the pink curve and the blue curve is β_i. By doing this, the transformed deterministic constraint can guarantee that the solutions satisfy the probabilistic constraint [Li *et al*. (2013)]. For more detail of demonstrations, we refer the interested readers to references [Li *et al*. (2013); Shan and Wang (2008)].

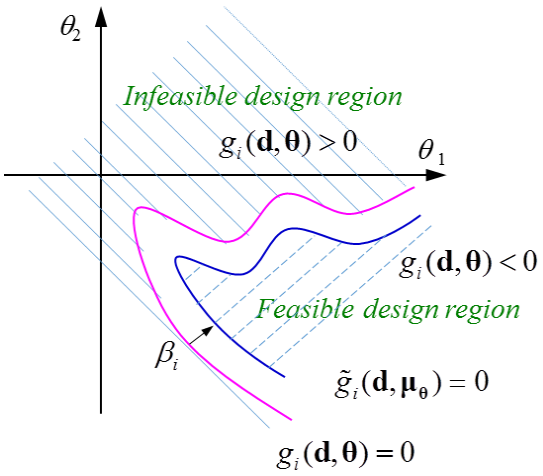

Figure 1. Illustration of the feasible design region.

2.2. *Formulation of approximating deterministic constraints*

In this section, the formulation of the transformed deterministic constraints as depicted in Figure 1 is presented. Let $g_i(\mathbf{d},\boldsymbol{\theta})$ and $\tilde{g}_i(\mathbf{d},\mu_\theta)$ are the limit-state function and the deterministic constraint function, respectively. Suppose that $\boldsymbol{\mu}_{\boldsymbol{\theta}}$ is any point on $\tilde{g}_i$, the most probable point (MPP) $\boldsymbol{\theta}_{\text{MPP}}$ corresponding to the point $\boldsymbol{\mu}_{\boldsymbol{\theta}}$ can be acquired by moving the point $\boldsymbol{\mu}_{\boldsymbol{\theta}}$ on $\tilde{g}_i$ back to g_i at least β_i.

According to reference [Shan and Wang (2008)], the MPP $\boldsymbol{\theta}_{\text{MPP}}$ on the failure surface in the standard normal space for the case $r_i \geq 0.5$ can be defined by

$$\theta^u_{j,\text{MPP}} = \beta_i \frac{\left(\partial g_i / \partial \theta^u_j\right)_\#}{\sqrt{\sum_j (\partial g_i / \partial \theta^u_j)^2_\#}}, j = 1,..,n,n+1,....,n+q. \tag{2}$$

where the subscript u denotes the standard normal distribution space and the derivatives $\left(\partial g_i / \partial \theta^u_j\right)_\#$ are evaluated at the MPP $\theta^u_{j,\text{MPP}}$.

The relationship of random parameters in the original design space and the normal standard space is depicted as follows

$$\theta^u_j = \frac{\theta_j - \mu_{\theta_j}}{\sigma_{\theta_j}} \tag{3}$$

where σ_{θ_j} is the deviation vector of θ_j.

From Eq. (3) we have

$$\frac{\partial g_i}{\partial \theta^u_j} = \frac{\partial g_i}{\partial \theta_j}\frac{\partial \theta_i}{\partial \theta^u_j} = \frac{\partial g_i}{\partial \theta_j}\sigma_{\theta_j} \tag{4}$$

From Eqs. (2), (3), and (4), the relationship between $\boldsymbol{\mu}_{\boldsymbol{\theta}}$ and its corresponding MPP point $\boldsymbol{\theta}_{\text{MPP}}$ in the original design space is denoted by

$$\theta_{j,\text{MPP}} = \mu_{\theta_j} + \beta_i \sigma_{\theta_j} \frac{\sigma_{\theta_j}\left(\partial g_i / \partial \theta_j\right)_\#}{\sqrt{\sum_j \left(\sigma_{\theta_j}\left(\partial g_i / \partial \theta^u_j\right)_\#\right)^2}} \tag{5}$$

where the derivatives $\left(\partial g_i / \partial \theta_j\right)_\#$ are evaluated at the MPP $\theta_{j,\text{MPP}}$ in the original space.

It has been shown in reference [Shan and Wang (2008)] that the derivatives $\left(\partial g_i / \partial \theta_j\right)_\#$ can be approximately assessed at μ_{θ_j} by substituting $\left(\partial g_i / \partial \theta_j\right)_\#$ with $\left(\partial g_i / \partial \mu_{\theta_j}\right)$. Thus, Eq. (5) can be rewritten by

$$\theta_{j,\text{MPP}} = \mu_{\theta_j} + \beta_i \sigma_{\theta_j} \frac{\sigma_{\theta_j}\partial g_i / \partial \mu_{\theta_j}}{\sqrt{\sum_j \left(\sigma_{\theta_j}\left(\partial g_i / \partial \mu_{\theta_j}\right)\right)^2}} \tag{6}$$

Once the MPP in the original design space $\boldsymbol{\theta}_{\text{MPP}}$ is determined**,** the feasible design domain of the RBDO problem can be denoted by approximating deterministic constraints as

$$\tilde{g}_i\left(\mathbf{d},\mu_\theta\right)=g_i\left(\mathbf{d},\mu_\theta+\sigma_\theta*\beta_i*\alpha\right)\le 0 \tag{7}$$

where $\boldsymbol{\alpha}=\dfrac{\boldsymbol{\sigma}_{\boldsymbol{\theta}}*\nabla_{\boldsymbol{\theta}}g_i(\boldsymbol{\mu}_{\boldsymbol{\theta}})}{\left\|\boldsymbol{\sigma}_{\boldsymbol{\theta}}*\nabla_{\boldsymbol{\theta}}g_i(\boldsymbol{\mu}_{\boldsymbol{\theta}})\right\|}$ is the approximately normalized gradient vector evaluated at $\boldsymbol{\mu}_{\boldsymbol{\theta}}$ on $g_i(\mathbf{d},\boldsymbol{\theta})$.

It is worth mentioning that the derivatives $\nabla_{\boldsymbol{\theta}}g_i(\boldsymbol{\mu}_{\boldsymbol{\theta}})$ can be easily acquired through the direct derivative of an explicit limit state function. Nevertheless, for the practical application problems, the structural behaviours are often analyzed by numerical methods, and hence the limit-state functions are often implicit. Therefore, to calculate the derivatives $\nabla_{\boldsymbol{\theta}}g_i(\boldsymbol{\mu}_{\boldsymbol{\theta}})$, the finite difference method, a numerical derivative method, is used.

3. NSGA-II algorithm

Unlike the single-objective optimization problem which provides only a single optimal solution, the multi-objective optimization problem will provide a set of points known as a Pareto-optimal set which represents the trade-off solutions between conflicting objectives. To obtain the Pareto-optimal solutions, a number of techniques have been proposed in the literature [Marler and Arora (2004)] in which the multi-objective evolutionary algorithms (MOEAs) such as NSGA-II [Deb *et al*. (2002)], SPEA-II [Zitzler *et al*. (2001)], and MOEA/D [Zhang and Li (2007)] gained much attention from the researchers due to their effectiveness and easy implementation. Among these attended MOEAs, the NSGA-II is considered as one of the most powerful methods. This algorithm is an improved version of NSGA [Srinivas and Deb (1994)] developed from the well-known genetic algorithm ([Liu *et al*. (2005); Liu and Chen (2001); Xu *et al*. (2002); Zheng *et al*. (2005)]) and non-dominated sorting concept by Goldberg [Goldberg (1989)]. In the past decade, the NSGA-II has been improved and widely applied in design optimization of various problems (see, for example, references [Dhanalakshmi *et al*. (2011); Kannan *et al*. (2009); Martínez-Vargas *et al*. (2016); Soyel *et al*. (2011)]) and also in design optimization of laminated composite plate structures [Honda *et al*. (2013); Pelletier and Vel (2006)]. In this paper, the NSGA-II algorithm is used to solve a multi-objective optimization problem related to the truss structures presented in section 6. The brief description of the algorithm is presented as follows.

(1) Generate an initial population P_0 with N random solutions.

(2) Create an offspring population Q_t using binary tournament selection based on the crowding-comparison operator, crossover and mutation performed on the parent population (P_t), where subscript "t" denotes the number of generations. The offspring population and its parent population are then combined to produce the entire population R_t.

(3) Perform a fast non-dominated sorting approach on the entire population R_t to identify different non-dominated fronts of objective functions F_1, F_2, etc.

(4) Create a new parent population (P_{t+1}) of size N from the obtained fronts (F_i).

(5) Repeat the process until the maximum number of iterations is reached.

For more details of the above procedure, the readers are encouraged to refer to the original paper [Deb *et al*. (2002)].

4. An effective couple method for solving reliability-based multi-objective optimization problems

By integrating the SLDM method in Section 2 into the NSGA-II algorithm in Section 3, the coupled method for solving reliability-based multi-objective optimization problems, namely SLDM-NSGA-II, is obtained. The flow chart of the proposed method is illustrated in Figure 2.

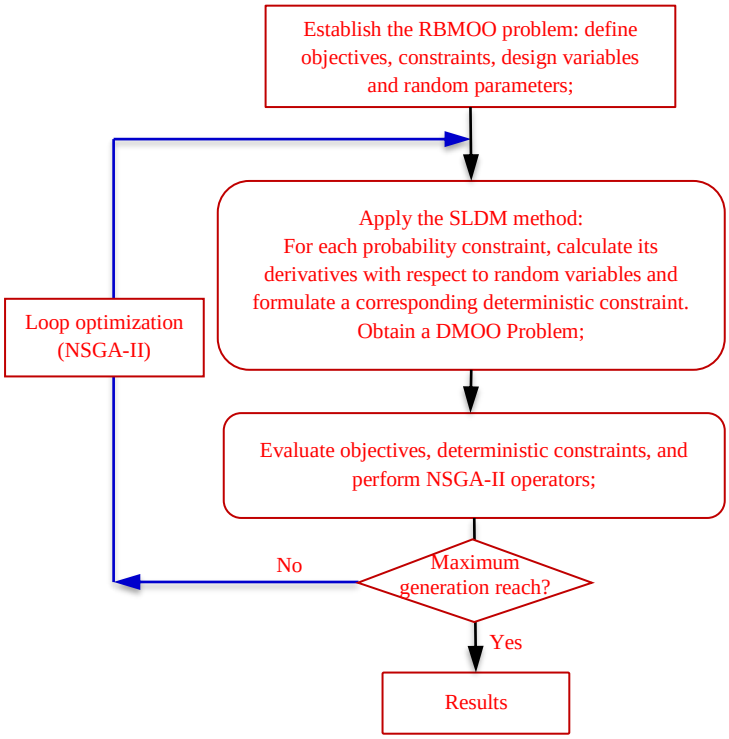

Figure 2. Flow chart of the SLDM-NSGA-II method.

5. Formulation of the deterministic and reliability-based multi-objective optimization problems for truss structures

In this section, the deterministic and reliability-based multi-objective optimization problems for truss structures are formulated. The objective functions are to minimize the

mass and minimize the displacement of trusses. The constraints include frequencies, displacement and stress of elements. For the deterministic multi-objective optimization (DMOO) problem, the design variable is the cross-sectional area of each element while the uncertainty of other parameters such as mass density, added mass, young modulus and applied force is not taken into account. For the reliability-based multi-objective optimization (RBMOO) problem, the cross-sectional areas of elements are considered as design variables and also random variables while the mass density, added mass, young modulus and applied force are considered as random variables that follow normal distribution.

The mathematical formulations of these problems are stated as follows:

(*i*) *The deterministic multi-objective optimization problem*

$$\begin{aligned} \min & \begin{cases} weight(\mathbf{A}) \\ disp_{\max}(\mathbf{A}) \end{cases} \\ \text{s.t.} \quad & \mathbf{A}^{\text{low}} \le \mathbf{A} \le \mathbf{A}^{\text{up}} \\ & disp_{\max}(\mathbf{A}) \le u^{\text{up}} \\ & stress_{\max}(\mathbf{A}) \le \sigma^{\text{up}} \\ & f_k \ge \underline{f}_k \qquad\qquad k \in \mathrm{Z}^+ \end{aligned} \tag{8}$$

(*ii*) *The reliability-based multi-objective optimization problem*

$$\begin{aligned} \min & \begin{cases} weight(\mu_{\mathbf{A}}, \mu_{\mathbf{Z}}) \\ disp_{\max}(\mu_{\mathbf{A}}, \mu_{\mathbf{Z}}) \end{cases} \\ \text{s.t.} \quad & \text{Prob.}\{g_l(\mathbf{A},\mathbf{Z}) \le 0\} \ge \Phi(\beta_l), \qquad l = 1,2,...,nc \\ & \mu_{\mathbf{A}}^{\text{low}} \le \mu_{\mathbf{A}} \le \mu_{\mathbf{A}}^{\text{up}} \\ \text{where} \quad & g_1(\mathbf{A},\mathbf{Z}) = disp_{\max}(\mathbf{A},\mathbf{Z}) - u^{\text{up}} \\ & g_2(\mathbf{A},\mathbf{Z}) = stress_{\max}(\mathbf{A},\mathbf{Z}) - \sigma^{\text{up}} \\ & g_l(\mathbf{A},\mathbf{Z}) = \underline{f}_k - f_k \qquad\qquad l \ge 3, \quad k \in \mathrm{Z}^+ \end{aligned} \tag{9}$$

where $weight(\mathbf{A}) = \rho \sum_{i=1}^{ne} l_i A_i$ is the mass of the truss structure; l_i is the length of the ith bar; $disp_{\max}(\mathbf{A}) = \max\left(\left|\mathbf{u}_j\right|\right)$ $j = 1,2,...,nn$ is the maximum displacement of the truss; $stress_{\max}(\mathbf{A}) = \max\left(\left|\sigma_m\right|\right)$, m = 1,2,…,ne; $\mathbf{u}_j$ is the displacements of the jth node; σ_m is the stress of the mth element; ne, nn and nc are the total number of bars, total number of nodes and number of constraints, respectively; $\underline{f}_k$ is the minimum allowable limit of the kth frequency; "low" and "up" denote the minimum and maximum allowable limits, respectively; $\mathbf{A}$ is the vector of random design variable consisting of cross-section areas of bars; $\mathbf{Z} = (\rho, W_0, P, E)$ is the vector of random parameters including mass density ρ, added mass W_0, concentrated load P and Modulus of Elasticity E; $\Phi\left(\beta_l\right)$ are desired

probabilities of constraint satisfaction; β_l is the target reliability index of the lth probabilistic constraint.

6. Numerical examples

In this section, the deterministic and reliability-based multi-objective optimization problems are solved for three truss structures including 10-bar, 72-bar and 200-bar trusses. These structures were previously solved by many researchers. However, they almost carried out the deterministic single-objective optimization problem subject to either static constraints or dynamic constraints. In the present paper, these truss structures are solved with two conflicting objectives subject to both static and dynamic constraints as introduced in Section 5. Furthermore, in each example, the reliability-based multi-objective optimization problem is studied.

All programming codes (including finite element analysis of the truss, the NSGA-II and SLDM-NSGA-II) are written in Matlab. The NSGA-II method and the SLDM-NSGA-II method are applied with a population size of 50 and a maximum generation of 500. It should be noted that with these given values, the number of function calls for the DMOO problems is 50×500. Meanwhile, for the RBMOO problems, by using the finite difference method, each random parameter (including random design variables) needs two function calls to evaluate the derivatives of constraints that are used for transforming probabilistic constraints into deterministic constraints. Therefore, the number of function calls for the RBMOO problems is $2\times n\times 50\times 500$, where n is the total number of random parameters. Furthermore, since the advantages of the SLDM method has been demonstrated to be much more effective compared to the double loop method and some other methods in previous studies [Li *et al*. (2013); Shan and Wang (2008)], and to avoid wordiness of the paper as well as the huge computational efforts, the integration of NSGA-II with the double loop method is not included in the investigation of the following examples. However, the reliability and efficiency of the proposed SLDM-NSGA-II are validated and compared with the DMOO results and some of the RBDO results which are available in the literature. In addition, to check whether the solutions by obtained SLDM-NSGA-II satisfy the reliability constraints or not, the first order reliability method (FORM) is used to evaluate the reliability of all obtained solutions, and some of them are extracted for comparison purposes.

6.1. *A 10-bar planar truss structure*

The 10-bar truss structure was previously studied by many researchers (see, for example, [Camp *et al*. (1998); Kaveh and Talatahari (2009); Lee and Geem (2004); Li *et al*. (2007)]). However, these studies have focused on single objective optimization with the goal of minimizing the weight of the structure subject to stress constraints. The geometry, boundary condition and loading condition of the 10-bar truss are illustrated in Figure 3. Four added masses are attached from nodes 1 to 4. The parameters of the truss are given in Table 1.

Table 1. Data for the 10-bar planar truss structure.

Parameter	Value (unit)
Modulus of elasticity E	6.895×10^{10} (N/m^2)
Material density ρ	2767 (kg/m^3)
Added mass W_0	454 (kg)
Force P	444.82×10^3 (N)
Minimum allowable limits of the first three frequencies	$\underline{f}_1$ = 7 (Hz), $\underline{f}_2$ = 15 (Hz), $\underline{f}_3$ = 20 (Hz)
Maximum allowable stress	172.375×10^6 (N/m^2)
Allowable range of cross-sections	0.6452 (cm^2) $\leq A_i \leq$ 225.80 (cm^2)

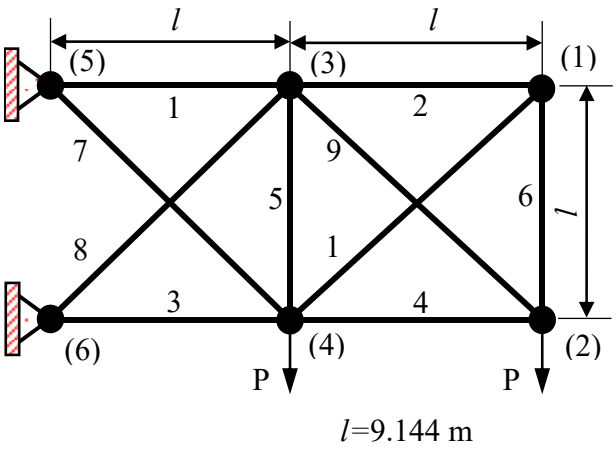

Figure 3. A 10-bar planar truss.

6.1.1. Deterministic multi-objective optimization

The DMOO of the 10-bar truss structure is examined with three different cases of constraints as follows. Case 1 includes displacement and stress constraints, and displacement constraint limit of 5.08 cm. Case 2 includes displacement, stress and frequency constraints and the displacement constraint limit of 5.08 cm. Case 3 includes displacement, stress and frequency constraints and the displacement constraint limit of 10.16 cm. The cross-section areas of all bar elements are considered as deterministic design variables. The allowable limits of variables and constraints are given in Table 1. Three deterministic Pareto optimal fronts: P1, P2 and P3 corresponding with three cases are shown in Figure 4. It can be seen from Figure 4 that P1 and P2 are very close to each other. However, the solutions in P2 satisfy the frequency constraints while the solutions in P1 do not satisfy the frequency constraints. Also, P3 is very close to P1 and P2 in a range of displacement less than 5.08 cm.

To evaluate the efficiency of the NSGA-II, some results (points A, B, C and D) in the deterministic Pareto optimal fronts in Figure 4 are extracted to compare with those obtained by Kaveh and Talatahari (2009), Li *et al*. (2007), Lee and Geem (2004) and

Camp *et al*. (1998) in Table 2. It can be seen from Table 2 that the weight at specific points of the Pareto optimal fronts, for example, points B and D, are nearly the same as those of other authors. Furthermore, the displacement and stress constraints of these results are satisfied. However, the frequency constraints of the present results are satisfied while the frequency constraints of reference results are violated.

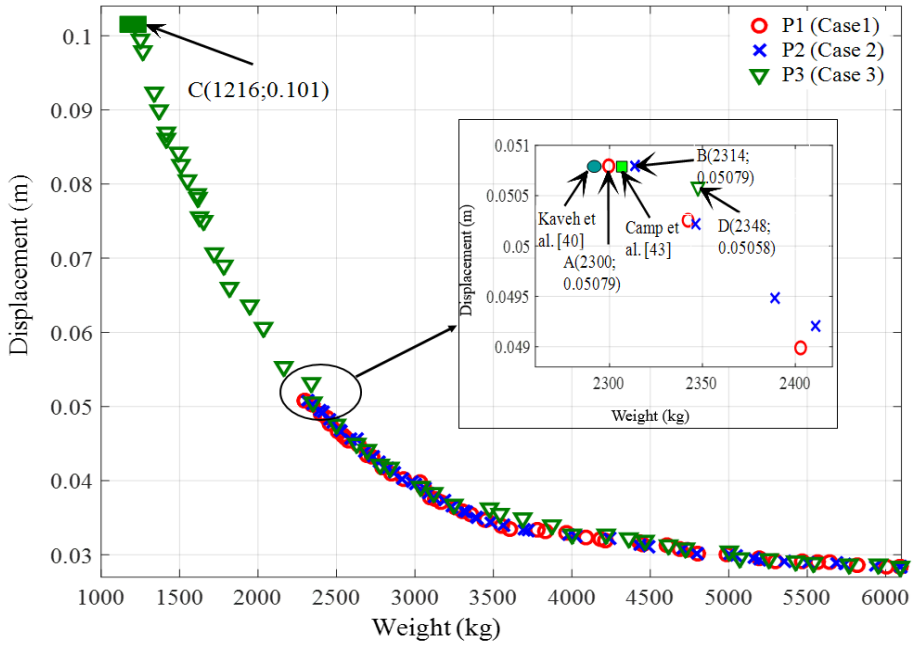

Figure 4. The deterministic Pareto-optimal solutions of the 10-bar planar truss structure with different cases of constraints.

Table 2. Comparison of deterministic results for the10-bar planar truss structure.

Design variable (cm^2)	Camp *et al.* (1998)	Lee and Geem (2004)	Li *et al.* (2007)	Kaveh and Talatahari (2009)	Present study (NSGA-II)			
	GA	HS	PSO	HPSACO	A(*)	B(**)	C(***)	D(***)
A_1	186.59	194.53	198.10	195.54	195.17	194.40	106.47	211.85
A_2	0.65	0.66	0.65	0.65	0.65	5.33	5.27	5.95
A_3	155.30	146.52	149.47	151.20	141.11	150.01	69.81	155.63
A_4	90.07	98.52	97.96	100.04	105.24	97.15	44.68	92.80
A_5	0.65	0.66	0.65	0.65	0.65	0.65	0.65	0.65
A_6	3.61	3.51	3.56	3.38	4.23	6.10	5.30	10.17
A_7	49.62	48.65	48.13	47.98	49.20	47.65	38.76	52.23
A_8	141.62	139.11	135.35	136.00	139.89	133.55	66.47	130.54

A_9	142.52	138.40	138.77	136.97	136.83	143.97	68.88	135.33
A_{10}	0.65	0.65	0.65	0.65	0.645	0.645	1.650	0.645
Weight (kg)	2302.60	2294.24	2295.62	2293.64	2300	2314	1216	2348
Displacement (cm)	5.08	5.08	5.08	5.08	5.0797	5.0797	10.159	5.058
Frequency	f_1=5.94	f_1= 5.96	f_1=5.93	f_1=5.93	f_1=5.92	f_1=11.2	f_1=9.2	f_1=11.89
	f_2=10.4	f_2= 10.3	f_2=10.4	f_2=10.3	f_2=10.78	f_2=15.02	f_2=15.1	f_2=15.76
	f_3=18.6	f_3= 18.5	f_3=18.5	f_3=18.3	f_3=19.14	f_3=20.23	f_3=20	f_3=21.29

Notes: $^{(*)}$: Case 1
$^{(**)}$: Case 2
$^{(***)}$: Case 3

6.1.2 Reliability-based multi-objective optimization

The RBMOO problem in Eq. (9) is adopted for the 10-bar truss configuration in this section. It is assumed that all random parameters are normally distributed with mean values given in Table 1 and the coefficient of variation (C.O.V.) of 0.05. Ten cross-section areas of the truss are considered as random design variables. The allowable range of these random design variables is provided in Table 1. The probability constraints are formulated from the constraints in Case 2 of the deterministic multi-objective optimization problem in Section 6.1.1. The reliability index of 3, causing a reliability of 99.87%, is investigated. In previous studies, the 10-bar truss structure has been studied for reliability-based single-objective optimization by several authors (see, for example [Shayanfar *et al*. (2014)] and [Lee *et al*. (2002)]) with the goal of minimizing the weight subject to displacement and stress constraints and the reliability index of 3.

The reliability-based Pareto optimal front is shown in Figure 5 in comparison with the deterministic Pareto optimal front. It can be observed that the reliability-based Pareto optimal front is almost overlapped by the deterministic Pareto optimal front. However, the range of the reliability-based Pareto optimal front is shorter and restricted to a safer design region compared with that of the deterministic Pareto optimal front. This is reasonable because the solutions of the reliability-based Pareto optimal front will have to move into the feasible design region where solutions have lower displacement and larger weight.

Several solutions of the deterministic and reliability-based Pareto optimal solutions (points A and B for deterministic optimization and point C for reliability-based optimization) are listed in Table 3 in comparison with those of Shayanfar *et al*. (2014) and Lee *et al*. (2002). It can be observed from Table 3 that the frequency constraints in reference solutions are violated while those of the points A, B and C are satisfied. In addition, some reliability indexes of point A and B are smaller than the given reliability index, for example, β_1 = 0.04, β_2 = 0.09, β_4= 0.03 and β_5= 0.34 for the case of point A and β_2= 0.06 and β_5= 0.94 for the case of point B. On the contrary, the reliability indexes for all constraints of the point C are satisfied.

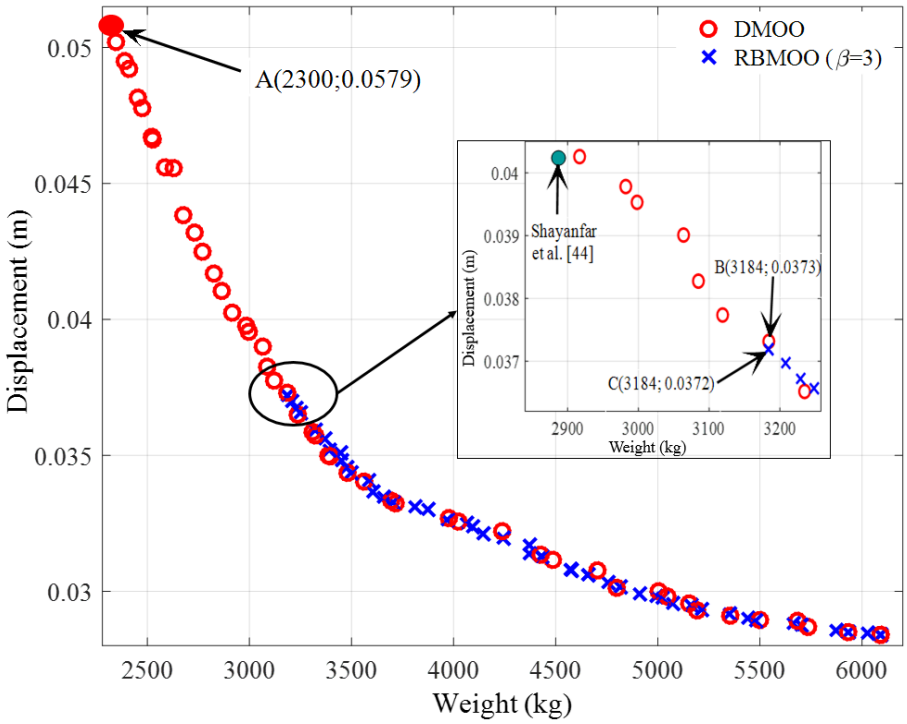

Figure 5. Comparison of the deterministic and reliability-based Pareto optimal fronts for the 10-bar planar truss structure.

Table 3. Comparison of deterministic and reliability-based results for the10-bar planar truss structure.

Design variable (cm^2)	Shayanfar *et al*. (2014)	Lee *et al*. (2002)	Present study		
	DLM-GA	TPB - β	DMOO		RBMOO
			A	B	C
A_1	221.64	248.47	194.40	225.81	225.43
A_2	0.65	0.65	5.33	7.32	7.04
A_3	191.51	173.43	150.01	220.77	215.34
A_4	169.53	123.04	97.15	123.36	137.69
A_5	0.65	0.65	0.65	0.65	0.65
A_6	0.65	0.65	6.10	26.36	8.95
A_7	21.53	39.87	47.65	51.83	66.91
A_8	182.94	176.46	133.55	207.26	197.47
A_9	168.64	175.04	143.97	202.88	204.04
A_{10}	0.65	0.65	0.645	0.645	0.645
Weight (kg)	2817.43	2787.17	2314	3184	3184
Displacement (cm)	-	-	5.0797	3.72	3.72
Frequency	f_1 = 5.12	f_1 = 5.12	f_1 = 11.2	f_1 = 13.38	f_1 = 12.68
	f_2 = 6.68	f_2 = 6.7	f_2 = 15.02	f_2 = 17.17	f_2 = 17.10
	f_3 = 13.12	f_3 = 16.43	f_3 = 20.23	f_3 = 20.70	f_3 = 22.31

			β_1= 0.04 (51.74%)	β_1= 2.96 (99.85%)	β_1= 3.00 (99.87%)
			β_2= 0.09 (53.46%)	β_2= 0.06 (52.26%)	β_2= 3.04 (99.88%)
β^{FORM}	3.060	2.999	β_3= 11.46 (100%)	β_3= 14.13 (100%)	β_3= 13.41 (100%)
			β_4= 0.03 (51.36%)	β_4= 3.26 (99.94%)	β_4= 3.11 (99.91%)
			β_5= 0.34 (63.36%)	β_5= 0.94 (82.68%)	β_5= 3.00 (99.87%)

The reliability-based Pareto optimal fronts of various reliability indexes are given in Figure 6. Here, we have investigated the reliability indexes which vary between 2 and 3.5, which corresponds to the reliabilities between 97.73% and 99.98%. It can be observed that the reliability-based Pareto optimal fronts almost match with each other. However, the larger the reliability index is, the narrower the range of Pareto optimal front becomes. This is reasonable because when the target reliability indexes become larger, the optimal solutions will have to move further from the constraint boundaries into the feasible design region to guarantee the larger target reliability index, and hence the range of weight will be shorter. The solutions having the smallest weight for each case of reliability index are listed in Table 4.

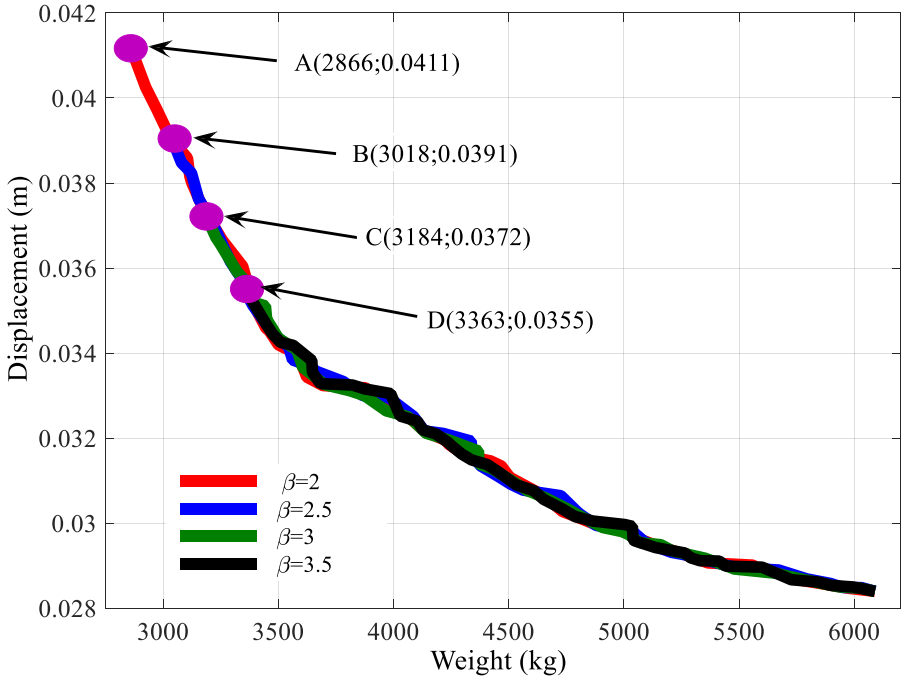

Figure 6. Reliability-based Pareto optimal fronts of the 10-bar planar truss structure with different reliability indexes.

Table 4. Comparison of the reliability-based results of the 10-bar planar truss structure with different reliability indexes.

Design variable (cm^2)		$\beta = 2$ (A)	$\beta = 2.5$ (B)	$\beta = 3$ (C)	$\beta = 3.5$ (D)
A_1		225.79	225.80	225.43	225.78
A_2		6.81	6.92	7.04	7.45
A_3		184.52	201.79	215.34	224.42
A_4		116.97	131.26	137.69	153.49
A_5		0.65	0.65	0.65	0.65
A_6		7.12	6.96	8.95	8.51
A_7		62.36	65.99	66.91	73.57
A_8		173.34	187.13	197.47	214.05
A_9		181.40	184.29	204.04	212.93
A_{10}		0.645	0.645	0.645	0.645
Weight (kg)		2866	3018	3184	3363
Displacement (cm)		4.11	3.91	3.72	3.55
β^{FORM}	β_1	2.00	2.50	3.00	3.50
	β_2	2.30	2.91	3.04	3.98
	β_3	12.71	12.84	13.41	13.47
	β_4	2.72	2.92	3.11	3.70
	β_5	2.43	2.52	3.00	3.50

6.2. *A 72-bar spatial truss structure*

The 72-bar spatial truss structure was studied by many researchers (see, for example, [Erbatur *et al*. (2000); Lee *et al*. (2002); Lee and Geem (2004); Perez and Behdinan (2007)]). In these studies, the truss was studied for single-objective (the weight of the truss) with displacement and stress constraints. The geometry and parameters of the truss are shown in Figure 7 and Table 5, respectively. Four masses are added into nodes 17, 18, 19 and 20 of the truss. Two separate load conditions are considered for designing of the truss as given in Table 6. The cross-section areas of the 72-bar's members of the truss are classified into 16 groups: (1) A_1-A_4, (2) A_5-A_{12}, (3) A_{13}-A_{16}, (4) A_{17}-A_{18}, (5) A_{19}-A_{22}, (6) A_{23}-A_{30}, (7) A_{31}-A_{34}, (8) A_{35}-A_{36}, (9) A_{37}-A_{40}, (10) A_{41}-$A4_8$, (11) A_{49}-A_{52}, (12) A_{53}-A_{54}, (13) A_{55}-A_{58}, (14) A_{59}-A_{66} (15), A_{67}-A_{70}, and (16) A_{71}-A_{72}.

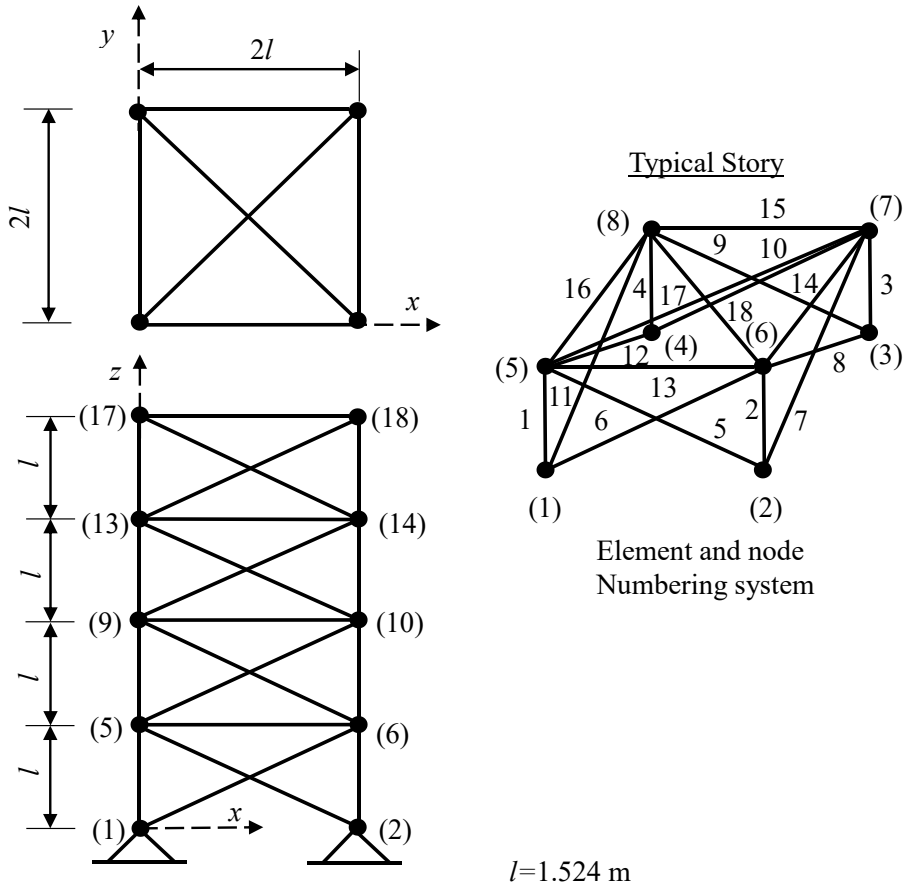

Figure 7. A 72-bar spatial truss structure.

Table 5: Data for the 72-bar spatial truss structure.

Parameters	Value (unit)
Modulus of elasticity E	6.895×10^{10} N/m^2
Material density ρ	2767 kg/m^3
Added mass W_0	2268 kg
Minimum allowable limits of the first and the third frequencies	$\underline{f}_1$ = 4 Hz, $\underline{f}_3$ = 6 Hz
Maximum allowable stress	172.375×10^6 N/m^2
Allowable range of cross-sections	0.6452 cm$^2 \leq A_i \leq$ 20.65 cm^2

Table 6: Load cases for the 72-bar spatial truss structure.

Node	Case 1			Case 2		
	P_x (kN)	P_y (kN)	P_z (kN)	P_x (kN)	P_y (kN)	P_z (kN)
17	22.25	22.25	-22.25	0.0	0.0	-22.25

18	0.0	0.0	0.0	0.0	0.0	-22.25
19	0.0	0.0	0.0	0.0	0.0	-22.25
20	0.0	0.0	0.0	0.0	0.0	-22.25

6.2.1 Deterministic multi-objective optimization

Similarly to the previous example in Section 6.1.1, three cases of constraints are carried out in this example. Case 1 considers only displacement and stress constraints with the maximum allowable displacement of 0.635 cm. Case 2 includes displacement, stress and frequency constraints with the maximum allowable displacement of 0.635 cm. Case 3 includes displacement, stress and frequency constraints with the maximum allowable displacement of 1.27 cm. The bar element cross-section areas of 16 groups are considered as deterministic design variables.

The deterministic Pareto optimal fronts of three cases are illustrated in Figure 8. It can be seen that P2 and P3 almost match with each other and they match partly with P1 in the safer design region. In addition, the maximum displacement of P2 and P3 equals to 0.503 that is less than the maximum allowable displacement. According to these results, it can be seen that the frequency constraint influences on the range of Pareto optimal front of the optimization problem.

Some solutions of the three deterministic Pareto optimal fronts are listed in Table 7 in comparison with those of the previous studies. It is worthy to note that the value of fitness functions at some points in P1, P2 and P3 are the same, however, the values of constraint functions at these points are different. The frequency constraints of the present solutions are satisfied while those of other authors are violated.

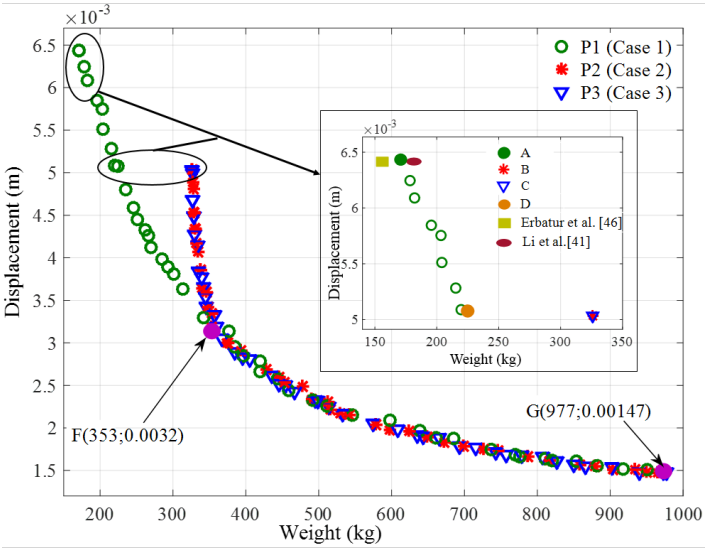

Figure 8. The deterministic Pareto-optimal solutions of the 72-bar spatial truss structure with different cases of constraints.

Table 7. Comparison of deterministic results for the 72-bar spatial truss structure.

Design variable (cm^2)		Erbatur *et al.* (2000)	Lee and Geem (2004)	Lee *et al.* (2002)	Perez and Behdinan (2007)	Present study (NSGA-II)			
						A(*)	D(*)	B(**)	C(***)
1	A_1-A_4	1.00	11.55	11.97	1.04	11.65	15.77	17.11	17.11
2	A_5-A_{12}	3.45	3.36	3.25	3.29	3.15	4.74	7.69	7.83
3	A_{13}-A_{16}	3.10	0.65	0.65	3.20	0.65	1.49	1.14	1.39
4	A_{17}-A_{18}	3.36	0.65	0.65	3.63	0.65	1.26	0.65	0.65
5	A_{19}-A_{22}	2.97	7.93	8.08	3.32	8.90	9.57	12.77	12.25
6	A_{23}-A_{30}	3.42	3.37	3.26	3.53	3.37	3.55	7.76	7.70
7	A_{31}-A_{34}	0.77	0.65	0.65	0.65	0.65	1.02	0.65	0.65
8	A_{35}-A_{36}	1.06	0.65	0.65	0.71	0.65	0.67	0.65	0.65
9	A_{37}-A_{40}	7.45	3.34	3.21	8.44	3.94	5.04	7.81	8.46
10	A_{41}-A_{48}	3.77	3.25	3.28	3.33	3.21	3.28	7.84	8.09
11	A_{49}-A_{52}	0.65	0.65	0.65	0.65	0.65	0.65	0.65	0.65
12	A_{53}-A_{54}	0.65	0.65	0.65	0.65	0.65	0.65	0.65	0.65
13	A_{55}-A_{58}	11.32	1.01	0.65	11.24	1.02	1.18	3.43	3.31
14	A_{59}-A_{66}	3.26	3.53	3.39	3.35	3.27	4.81	8.50	8.12
15	A_{67}-A_{70}	0.68	2.85	2.54	0.65	3.18	3.59	0.65	0.65
16	A_{71}-A_{72}	0.68	4.45	3.45	0.65	3.40	7.82	0.65	0.65
Weight (kg)		174.98	172.04	167.67	173.23	171.22	224.57	325.86	325.86
Displacement (cm)		-	-	-	-	0.643	0.508	0.503	0.503
Frequency		f_1 = 1.7 f_3 = 4.0	f_1 = 2.8 f_3 = 3.9	f_1 = 2.7 f_3 = 3.9	f_1 = 1.8 f_3 = 3.9	f_1 = 2.8 f_3 = 3.8	f_1 = 3.12 f_3 = 4.25	f_1 = 4.0 f_3 = 6.0	f_1 = 4.0 f_3 = 6.0

Notes: (*): Case 1
(**): Case 2
(***): Case 3

6.2.2 Reliability-based multi-objective optimization

The RBMOO problem in Eq. (9) is solved for the 72-bar truss structure. Five probability constraints formulating for Case 2 in Section 6.2.1 are considered. All random parameters obey normal distribution with the mean values in Table 5 and C.O.V. of 0.05. Reliability indexes of the optimization problem are chosen to be 3. The bar element cross-section areas of the 16 groups are considered as random design variables. The allowable range of these random design variables is given in Table 5.

The result of this problem is shown in Figure 9 in comparison with those of Case 2 in Section 6.2.1. It is seen that unlike the 10-bar truss structure, the reliability-based Pareto optimal front almost matches with deterministic Pareto optimal front in the safer design region and separates in the remainder. Several solutions in the Pareto optimal fronts are listed in Table 8.

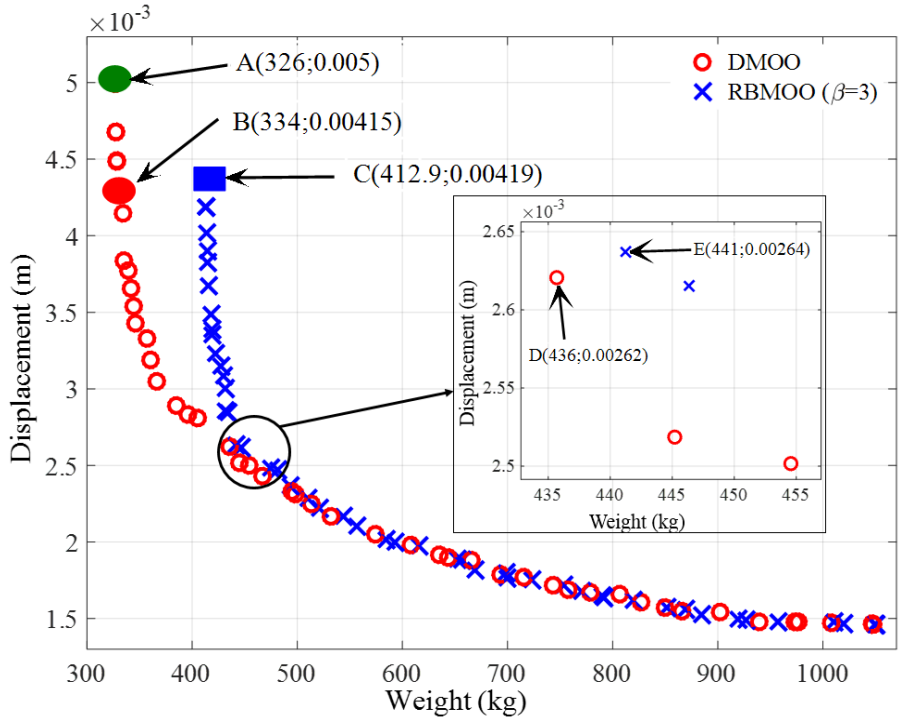

Figure 9. Comparison of the deterministic and reliability-based Pareto optimal fronts for the 72-bar spatial truss structure.

Table 8. Comparison of deterministic and reliability-based results for the 72-bar spatial truss structure.

Design variable (cm^2)		DMOO			RBMOO	
		A	B	D	C	E
1	A_1-A_4	17.11	17.28	20.65	20.51	20.64
2	A_5-A_{12}	7.69	7.70	10.01	9.57	9.59
3	A_{13}-A_{16}	1.14	1.17	1.15	2.13	2.13
4	A_{17}-A_{18}	0.65	0.65	0.65	0.65	0.65
5	A_{19}-A_{22}	12.77	12.80	16.12	16.86	20.65
6	A_{23}-A_{30}	7.76	7.76	11.90	10.20	10.32
7	A_{31}-A_{34}	0.65	0.65	0.67	0.65	0.77
8	A_{35}-A_{36}	0.65	0.65	0.66	0.65	0.88
9	A_{37}-A_{40}	7.81	7.85	10.03	10.44	11.02
10	A_{41}-A_{48}	7.84	8.27	7.09	10.65	10.52
11	A_{49}-A_{52}	0.65	0.68	0.65	0.65	0.65
12	A_{53}-A_{54}	0.65	0.65	3.11	0.65	0.65
13	A_{55}-A_{58}	3.43	3.52	2.75	4.11	2.39
14	A_{59}-A_{66}	8.50	8.50	7.95	10.02	10.36
15	A_{67}-A_{70}	0.65	0.72	8.16	0.65	3.45
16	A_{71}-A_{72}	0.65	2.28	11.28	0.75	5.18
Weight (kg)		325.86	334	436	412.9	441
Displacement (cm)		0.503	0.415	0.26	0.419	0.26
Frequency		f_1 = 4.0	f_1 = 4.02	f_1 = 4.29	f_1 = 4.50	f_1 = 4.51
		f_3 = 6.0	f_3 = 6.04	f_3 = 6.33	f_3 = 6.76	f_3 = 6.78
β^{FORM}		β_1= 2.25 (98.77%)	β_1= 4.20 (99.99%)	β_1= 8.92 (100%)	β_1= 4.10 (99.99%)	β_1= 8.87 (100%)

β_2= 11.88 (100%)	β_2= 11.96 (100%)	β_2= 11.53 (100%)	β_2= 14.19 (100%)	β_2= 9.59 (100%)
β_3= 0.00 (42.91%)	β_3= 0.00 (48.26%)	β_3= 1.77 (96.13%)	β_3= 3.00 (99.87%)	β_3= 3.05 (99.88%)
β_4= 0.00 (43.11%)	β_4= 0.004 (50.16%)	β_4= 1.30 (90.24%)	β_4= 3.00 (99.87%)	β_4= 3.10 (99.90%)

The Pareto optimal fronts for various reliability indexes of the 72-bar spatial truss structure are depicted in Figure 10. The results show that the larger the reliability index is, the shorter the Pareto optimal front becomes. Also, the Pareto optimal fronts are separate in the range of the weight less than 500 kg. Some solutions having minimum weight and maximum displacement for various reliability indexes are shown in Table 9.

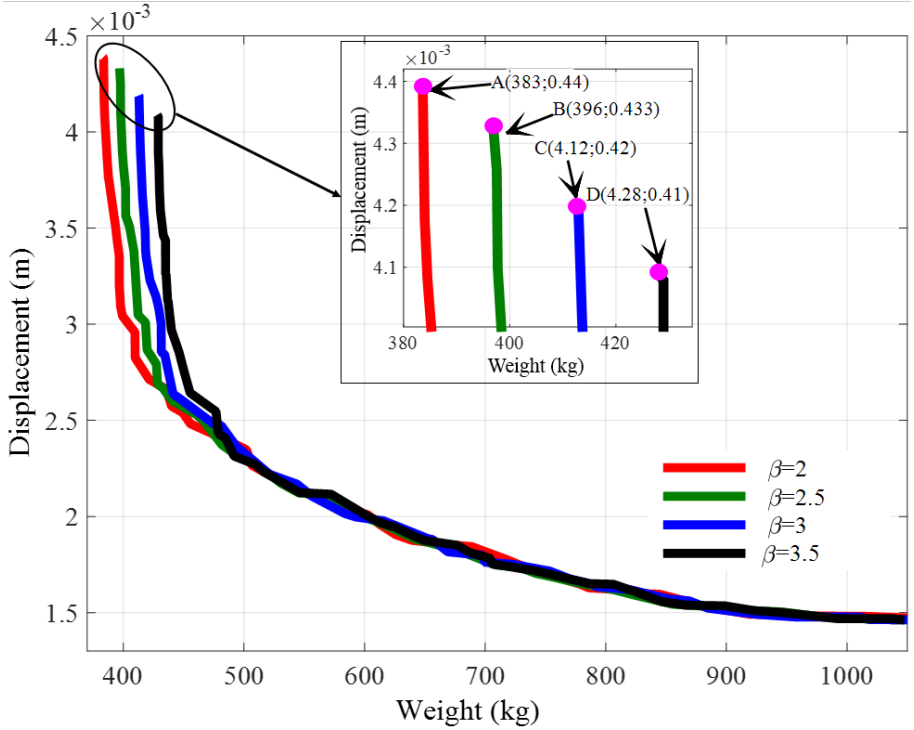

Figure 10. Reliability-based Pareto optimal fronts of the 72-bar spatial truss structure with different reliability indexes.

Table 9. Comparison of the reliability-based results of the 72-bar spatial truss structure with different reliability indexes.

Design variable (cm^2)		β = 2 (A)	β = 2.5 (B)	β = 3 (C)	β = 3.5 (D)
1	A_1-A_4	19.27	20.59	20.51	20.64
2	A_5-A_{12}	9.47	10.03	9.57	10.52
3	A_{13}-A_{16}	1.82	1.91	2.13	2.21
4	A_{17}-A_{18}	0.65	0.65	0.65	0.65
5	A_{19}-A_{22}	15.45	15.73	16.86	17.45

Design variable (cm^2)		$\beta = 2$ (A)	$\beta = 2.5$ (B)	$\beta = 3$ (C)	$\beta = 3.5$ (D)
6	A_{23}-A_{30}	9.52	9.88	10.20	10.20
7	A_{31}-A_{34}	0.65	0.65	0.65	0.65
8	A_{35}-A_{36}	0.65	0.65	0.65	0.65
9	A_{37}-A_{40}	9.14	9.31	10.44	11.14
10	A_{41}-A_{48}	9.58	9.37	10.65	10.41
11	A_{49}-A_{52}	0.65	0.65	0.65	0.65
12	A_{53}-A_{54}	0.65	0.65	0.65	0.65
13	A_{55}-A_{58}	4.35	4.31	4.11	4.69
14	A_{59}-A_{66}	8.89	9.59	10.02	10.82
15	A_{67}-A_{70}	0.65	0.65	0.65	0.65
16	A_{71}-A_{72}	0.82	0.74	0.75	0.77
Weight (kg)		383.28	396.86	412.85	428.00
Displacement (cm)		0.44	0.43	0.42	0.41
β^{FORM}	β_1	3.61	3.76	4.10	4.36
	β_2	14.02	13.68	14.19	14.59
	β_3	2.01	2.50	3.00	3.50
	β_4	2.01	2.50	3.00	3.50

6.3. *A 200-bar planar truss structure*

In the previous works, the 200-bar truss structure was studied for single-objective optimization with various cases of constraints. For example, Kaveh and Talatahari (2009), Lamberti (2008), Sonmez (2011), and Lee and Geem (2004) minimized the weight of the truss structure subject to stress constraints. Pholdee and Bureerat (2012), (2013) minimized the weight of the truss subject to displacement constraints. Farshchin *et al*. (2016), Kaveh and Ilchi Ghazaan (2015) and Khatibinia and Sadegh Naseralavi (2014) optimized the weight of the truss with frequency constraints. The geometry, node numbering, material numbering and group numbers of the 200-bar truss are shown in Figure 11. The 200 bars of the truss structure are categorized into 29 groups as given in Table 10. The truss structure is subjected to three loading conditions: (1) 4.45 kN acting in the positive *x* direction at nodes 1, 6, 15, 20, 29, 34, 43, 48, 57, 62, and 71; (2) 44.5 kN acting in the negative *y* direction at nodes 1, 2, 3, 4, 5, 6, 8, 10, 12, 14, 15, 16, 17, 18, 19, 20, 22, 24, 26, 28, 29, 30, 31, 32, 33, 34, 36, 38, 40, 42, 43, 44, 45, 46, 47, 48, 50, 52, 54, 56, 57, 58, 59, 60, 61, 62, 64, 66, 68, 70, 71,72, 73,74, and 75; (3) cases 1 and 2 are combined together. Five added masses are attached in nodes 1, 2, 3, 4 and 5. The parameters of the truss structure are provided in Table 11.

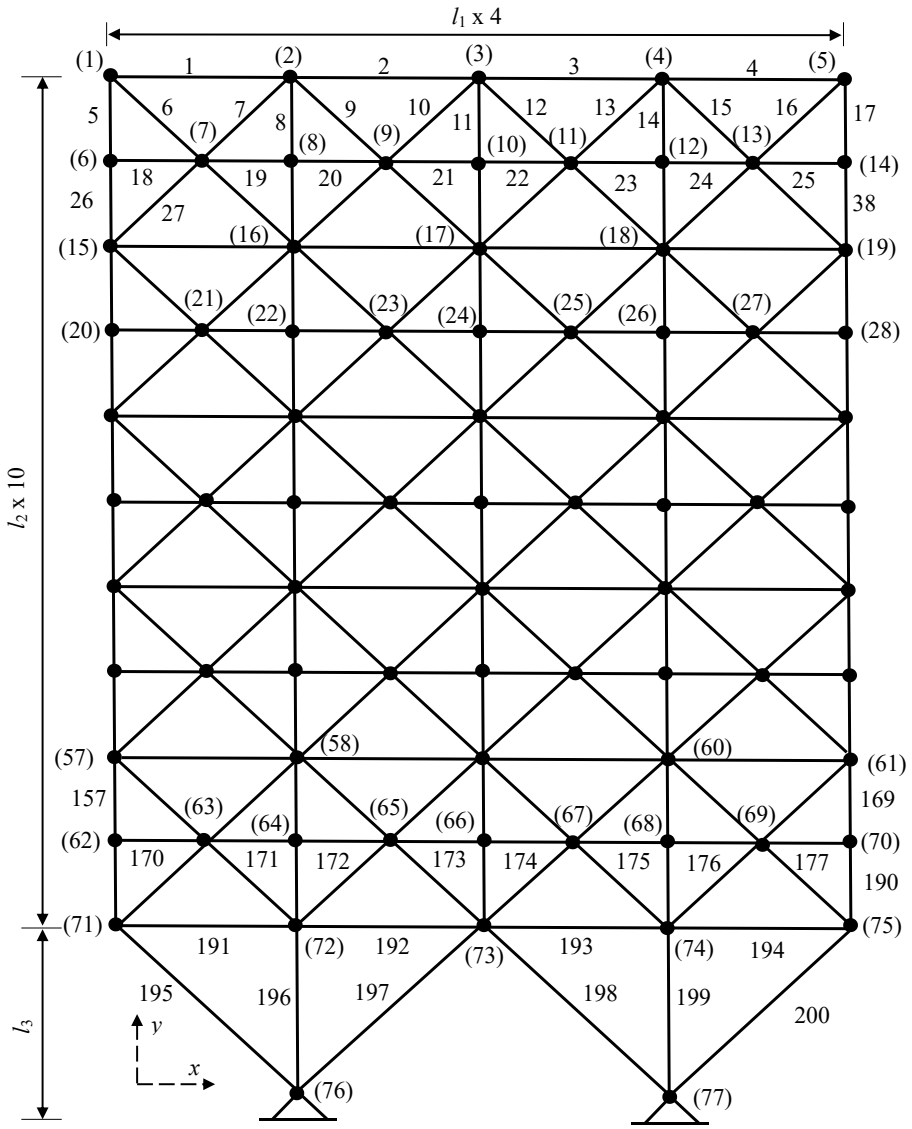

l_1=6.096 m, l_2=3.657 m, l_3=9.144 m

Figure 11. A 200-bar planar truss structure.

Table 10. Element groups for the 200-bar planar truss structure.

Group	Elements	Group	Elements
1	1 2 3 4	16	82 83 85 86 88 89 91 92 103 104 106 107 109 110 112 113
2	5 8 11 14 17	17	115 116 117 118

Group	Elements	Group	Elements
3	19 20 21 22 23 24	18	119 122 125 128 131
4	18 25 56 63 94 101 132 139 170 177	19	133 134 135 136 137 138
5	26 29 32 35 38	20	140 143 146 149 152
6	6 7 9 10 12 13 15 16 27 28 30 31 33 34 36 37	21	120 121 123 124 126 127 129 130 141 142 144 145 147 148 150 151
7	39 40 41 42	22	153 154 155 156
8	43 46 49 52 55	23	157 160 163 166 169
9	57 58 59 60 61 62	24	171 172 173 174 175 176
10	64 67 70 73 76	25	178 181 184 187 190
11	44 45 47 48 50 51 53 54 65 66 68 69 71 72 74 75	26	158 159 161 162 164 165 167 168 179 180 182 183 185 186 188 189
12	77 78 79 80	27	191 192 193 194
13	81 84 87 90 93	28	195 197 198 200
14	95 96 97 98 99 100	29	196 199
15	102 105 108 111 114		

Table 11. Data for the 200-bar planar truss structure.

Parameters	Value (unit)
Modulus of elasticity E	2.06×10^{11} (N/m^2)
Material density ρ	7933.410 (kg/m^3)
Added mass W_0	100 (kg)
Minimum allowable limits of the first three frequencies	$\underline{f}_1$ = 5 (Hz), $\underline{f}_2$ = 10 (Hz), $\underline{f}_3$ = (15 Hz)
Maximum allowable stress	68.95×10^6 (N/m^2)
Allowable range of cross-sections	0.6452 (cm^2) $\leq A_i \leq$ 129.03 (cm^2)

6.3.1 Deterministic multi-objective optimization

Similar to the previous examples, three cases of constraints are carried out in this example. Case 1 considers only displacement and stress constraints with the maximum allowable displacement of 1.5 cm. Case 2 includes displacement, stress and frequency constraints with the maximum allowable displacement of 1.5 cm. Case 3 includes displacement, stress and frequency constraints with the maximum allowable displacement of 3 cm. The bar element cross-section areas of 29 groups are deterministic design variables.

The deterministic Pareto optimal fronts of the optimization problem are shown in Figure 12. It can be seen that these results are not similar to those in the 10-bar planar and 72-bar spatial truss structures. Three Pareto optimal fronts almost match with each other

although the constraints are different for each case. In addition, the maximum displacement of the Pareto optimal front of Case 3 is less than the maximum allowable displacement.

Some specific solutions in Figure 12 are provided in Table 12 in comparison with the studies of Kaveh and Talatahari (2009); Lamberti (2008); Lee and Geem (2004); and Sonmez (2011).

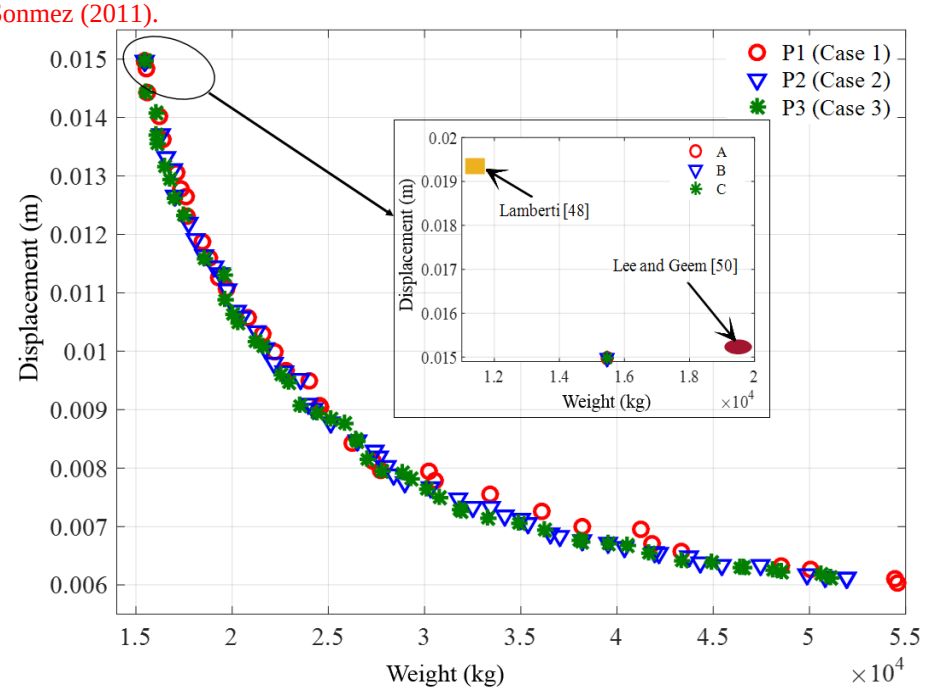

Figure 12. The deterministic Pareto-optimal solutions of the 200-bar planar truss structure with different cases of constraints.

Table 12. Comparison of deterministic results for the 200-bar planar truss structure.

Design variables (cm^2)	Lamberti (2008)	Sonmez (2011)	Lee and Geem (2004)	Kaveh and Talatahari (2009)	Present study		
	CMLPSA	ABC-AP	PSO	HPSACO	A(*)	B(**)	C(***)
1	0.95	0.67	5.17	0.67	1.23	1.23	1.23
2	6.06	6.11	15.50	5.93	7.33	7.33	7.33
3	0.65	0.67	28.01	0.78	0.65	0.65	0.65
4	0.65	0.73	36.76	0.65	0.76	0.76	0.76
5	12.52	12.59	25.51	12.04	17.00	17.00	17.00
6	1.91	1.89	3.84	1.82	0.65	0.65	0.65
7	0.65	0.69	36.18	0.65	2.03	2.03	2.03
8	20.03	20.16	59.33	19.15	25.71	25.71	25.71
9	0.65	0.69	29.12	0.65	0.65	0.65	0.65
10	26.48	26.64	29.69	25.46	28.73	28.73	28.73
11	2.60	2.74	3.58	2.41	5.51	5.51	5.51

Design variables (cm^2)	Lamberti (2008)	Sonmez (2011)	Lee and Geem (2004)	Kaveh and Talatahari (2009)	Present study		
	CMLPSA	ABC-AP	PSO	HPSACO	A(*)	B(**)	C(***)
12	1.23	0.67	120.98	2.90	4.21	4.21	4.21
13	35.02	35.36	38.67	32.00	44.61	44.61	44.61
14	0.65	0.68	0.65	6.93	2.13	2.13	2.13
15	41.48	41.84	52.62	38.57	51.60	51.60	51.60
16	3.70	3.61	1.75	5.07	7.26	7.26	7.26
17	0.86	1.18	71.95	4.76	2.04	2.04	2.04
18	51.43	51.90	45.98	47.62	65.39	65.39	65.39
19	0.65	0.66	28.81	4.31	0.83	0.83	0.83
20	57.89	58.28	59.13	53.55	75.99	75.99	75.99
21	4.55	5.06	17.82	7.72	7.29	7.29	7.29
22	2.71	4.84	3.58	6.45	2.00	2.00	2.00
23	70.09	72.94	104.29	69.85	88.54	88.54	88.54
24	0.65	1.42	3.21	0.65	13.90	13.90	13.90
25	76.52	79.19	104.68	75.47	94.50	94.50	94.50
26	6.67	9.07	6.48	8.85	15.10	15.10	15.10
27	43.11	33.29	23.29	31.95	43.89	43.89	43.89
28	69.75	64.47	53.99	56.77	86.22	86.22	86.22
29	89.32	94.85	100.41	94.61	116.55	116.55	116.55
Weight (kg)	11542.92	11582.05	19995.19	11410.914	15470.20	15470.20	15470.20
Displacement (cm)	1.93	1.93	1.57	2.00	1.497	1.497	1.497
Frequency	f_1 = 5.7 f_2 =15.8 f_3 =20.6	f_1 = 5.7 f_2 =16.0 f_3 =20.8	f_1 = 3.38 f_2 =11.3 f_3 =17.5	f_1 = 5.8 f_2 =15.7 f_3 =21.5	f_1 = 6.11 f_2 =13.87 f_3 =22.19	f_1 = 6.11 f_2 =13.87 f_3 =22.19	f_1 = 6.11 f_2 =13.87 f_3 =22.19

Notes: (*): Case 1
(**): Case 2
(***): Case 3

6.3.2 Reliability-based multi-objective optimization

In this section, the RBMOO problem as presented in Eq. (9) is solved for the 200-bar truss. All random parameters obey the normal distribution. The mean values of these parameters are given in Table 11, with C.O.V. of 0.05. The probability constraints of a single displacement, single stress and three frequencies are formulated similarly as the Case 2 in the Section 6.3.1. Reliability indexes of the optimization problem are chosen to be β = 2.5 corresponding with the probability of safety of 99.38%. The bar element cross-section areas of 29 groups are random design variables having a normal distribution with C.O.V. of 0.05. The allowable ranges of these random design variables are given in Table 11.

The results of this problem are shown in Figure 13 in comparison with those of Case 2 for the DMOO problem in Section 6.3.1. It can be seen from Figure 13 that similar to the previous results, the reliability-based Pareto optimal front is nearly overlapped by the deterministic Pareto front. However, the range of the reliability-based Pareto optimal front is shorter and restricted to a safer design region compared with that of the

deterministic Pareto optimal front. Several solutions having the smallest weight of the Pareto optimal fronts are shown in Table 13.

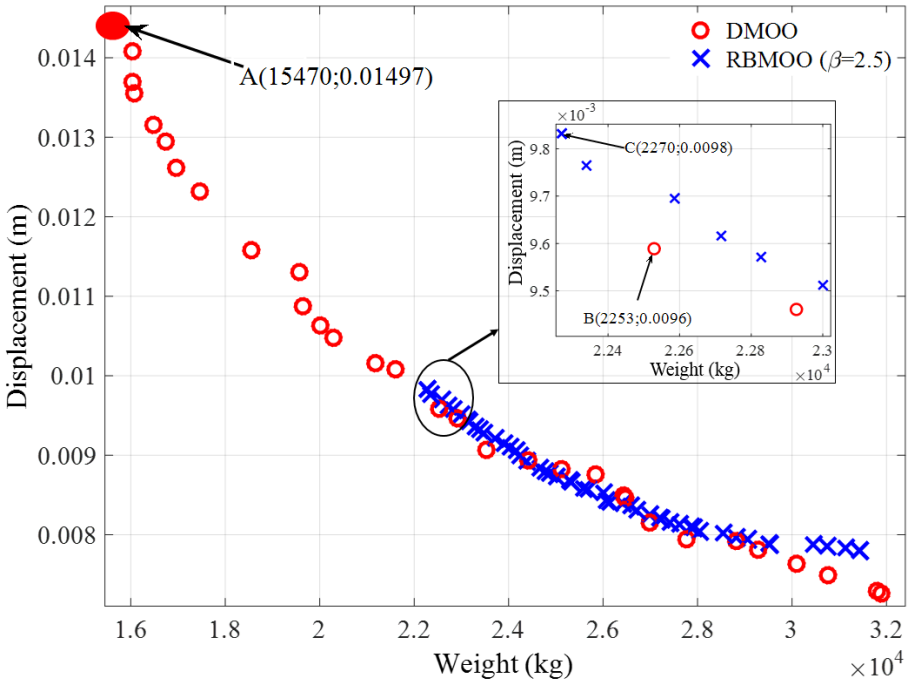

Figure 13. Comparison of the deterministic and reliability-based Pareto optimal fronts for the 200-bar planar truss structure.

Table 13. Comparison of deterministic and reliability-based results for the 200-bar planar truss structure.

Design variables (cm^2)	DMOO		RBMOO
	A	B	C
1	1.23	3.51	3.14
2	7.33	24.68	19.89
3	0.65	0.66	8.51
4	0.76	3.71	2.31
5	17.00	63.71	47.34
6	0.65	2.90	0.65
7	2.03	6.64	0.65
8	25.71	32.38	65.18
9	0.65	0.65	6.83
10	28.73	69.04	57.71
11	5.51	6.70	10.06
12	4.21	0.65	6.05
13	44.61	69.19	72.88
14	2.13	1.72	0.65
15	51.60	85.40	80.12
16	7.26	7.08	14.12

Design variables (cm^2)	DMOO		RBMOO
	A	B	C
17	2.04	1.58	0.74
18	65.39	116.46	80.79
19	0.83	0.79	0.65
20	75.99	107.39	95.29
21	7.29	10.25	12.45
22	2.00	0.65	1.98
23	88.54	107.03	100.91
24	13.90	6.77	5.18
25	94.50	113.76	108.96
26	15.10	11.74	14.46
27	43.89	97.07	81.92
28	86.22	129.03	128.08
29	116.55	128.12	128.99
Weight (kg)	15470.20	22528.90	22270.10
Displacement (cm)	1.497	0.96	0.98
Frequency	f_1=6.11 f_2=13.87 f_3=22.19	f_1=5.41 f_2=16.38 f_3=21.98	f_1=5.55 f_2=12.56 f_3=23.23
β^{FORM}	β_1=0.06 (52.39%) β_2=0.05 (51.99%) β_3=5.59 (100%) β_4=8.32 (100%) β_5=9.56 (100%)	β_1=4.43 (99.99%) β_2=2.26 (98.81%) β_3=2.38 (99.13%) β_4=11.85 (100%) β_5=8.62 (100%)	β_1=4.21 (99.99%) β_2=2.50 (97.79%) β_3=2.93 (99.83%) β_4=5.75 (100%) β_5=10.69 (100%)

The reliability-based Pareto optimal fronts for various reliability indexes are illustrated in Figure 14. Similar to the previous examples, the reliability index influences on the range of the Pareto optimal fronts, i.e. the range of the Pareto optimal fronts becomes narrower when the reliability index is larger. The solutions having the lowest weight of Pareto optimal fronts for each reliability index are shown in Table 14. As can be seen in Table 14 that the reliability indexes computed by FORM algorithm are greater than or equal the defined reliability index.

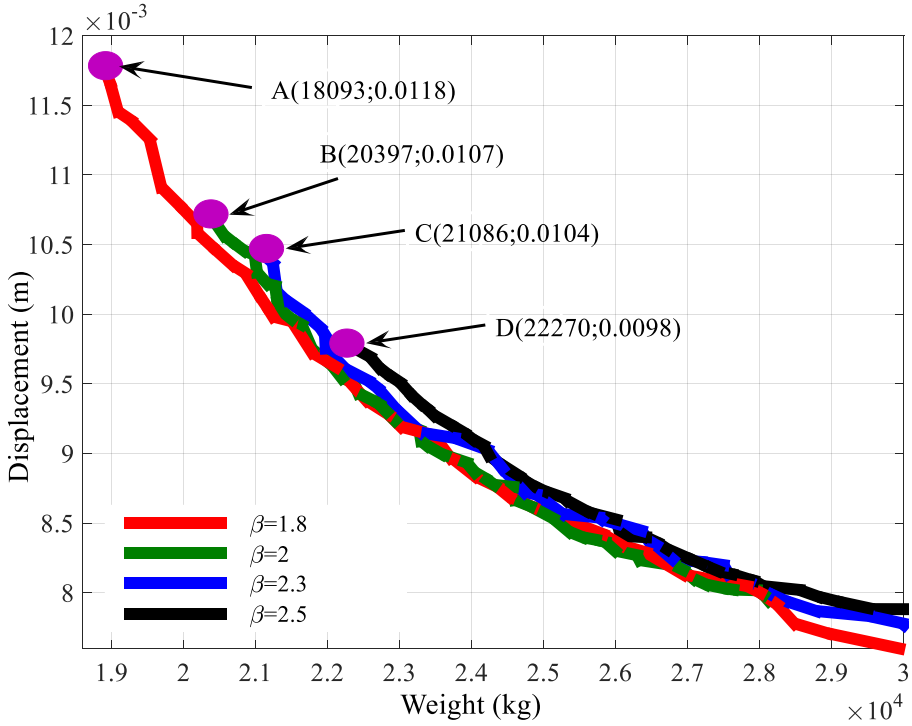

Figure 14. Reliability-based Pareto optimal fronts of the 200-bar planar truss structure with different reliability indexes.

Table 14. Comparison of the reliability-based results of the 200-bar planar truss structure with different reliability indexes.

Design variables (cm^2)	β = 1.8 (A)	β = 2.0 (B)	β = 2.3 (C)	β = 2.5 (D)
1	0.70	1.32	0.65	3.14
2	17.30	34.27	13.12	19.89
3	0.65	0.65	13.43	8.51
4	1.81	1.12	1.30	2.31
5	29.00	36.90	32.80	47.34
6	1.00	0.65	0.65	0.65
7	5.99	0.65	6.20	0.65
8	27.54	40.59	41.88	65.18
9	0.65	0.65	2.88	6.83
10	36.73	71.71	73.87	57.71
11	7.41	5.07	6.61	10.06
12	1.54	18.34	0.65	6.05
13	50.92	53.80	76.78	72.88
14	0.65	1.68	0.65	0.65
15	59.96	70.93	66.23	80.12
16	8.50	8.69	7.56	14.12

Design variables (cm^2)		β = 1.8 (A)	β = 2.0 (B)	β = 2.3 (C)	β = 2.5 (D)
17		3.35	8.09	0.65	0.74
18		73.49	72.73	106.86	80.79
19		0.65	0.65	0.65	0.65
20		85.23	79.77	96.67	95.29
21		10.11	10.79	8.61	12.45
22		5.15	2.35	5.73	1.98
23		100.13	98.51	100.90	100.91
24		0.65	0.65	0.65	5.18
25		117.61	108.48	107.55	108.96
26		9.44	10.57	15.68	14.46
27		70.79	101.79	89.13	81.92
28		126.23	115.57	118.93	128.08
29		126.01	127.74	129.03	128.99
Weight (kg)		18903.2	20397.2	21086.5	22270.1
Displacement (cm)		1.18	1.07	1.04	0.98
β^{FORM}	β_1	2.34	3.38	3.56	4.21
	β_2	1.90	2.06	2.44	2.50
	β_3	5.27	2.36	3.12	2.93
	β_4	10.08	4.93	6.57	5.75
	β_5	6.55	5.77	7.84	10.69

7. Conclusions

In this article, an effective couple method is proposed for solving the reliability-based multi-objective optimization problems of truss structure subject to both static and dynamic constraints. In the optimization problems, the conflicting objective functions are to minimize the weight and minimize the displacement of truss structures under uncertainties in structural design variables, loading conditions and material parameters. The design variables are cross-section areas of the bars. The couple method is proposed by integrating a single-loop deterministic method (SLDM) into the NSGA-II algorithm to give the called SLDM-NSGA-II. Thanks to the advantage of SLDM, the probabilistic constraints are treated as approximate deterministic constraints. And therefore the reliability-based multi-objective optimization problems can be transformed into the deterministic multi-objective optimization problems of which the computational cost is reduced significantly. To illustrate the efficiency and robustness of the proposed method, three benchmark-type truss structures including a 10-bar planar truss, a 72-bar spatial truss and a 200-bar planar truss are studied. The influence of various parameters on the reliability-based Pareto optimal fronts is also demonstrated. Based on the obtained results, some concluding remarks can be withdrawn as follows:

i) The frequency constraint has certain influences on the Pareto optimal front of the truss structures. The level of the influence depends on the specific truss structures. In addition, the allowable limit of displacement also effects on the Pareto optimal fronts for some truss structures.

ii) The reliability-based Pareto optimal front is almost overlapped by

deterministic Pareto optimal front. However, the range of the reliability-based Pareto optimal front is shorter and restricted to a safer design region compared with that of the deterministic Pareto optimal front.

iii) The reliability index effects on the range of the Pareto optimal fronts. The different reliability-based Pareto optimal fronts almost match with each other. However, the range of Pareto optimal fronts becomes narrower when the reliability index is larger. For some truss structures, it also effects on the form of the Pareto optimal front.

It can be seen that various parameters effect on Pareto optimal fronts and for each truss structure the effect of these parameters is different. As a result, the reliability-based multi-objective optimization should be taken into account for each truss structure to get the optimal design. In the future, the proposed approach can be extended to various types of structures.

Acknowledgments

This research is funded by Vietnam National Foundation for Science and Technology Development (NAFOSTED) under grant number 107.02-2017.08.

References

Camp, C., Pezeshk, S. and Cao, G. (1998). Optimized design of two-dimensional structures using a genetic algorithm. *Journal of Structural Engineering*, **124**, 5, pp. 551–559.

Coello, C. A. and Christiansen, A. D. (2000). Multiobjective optimization of trusses using genetic algorithms. *Computers & Structures*, **75**, 6, pp. 647–660.

Deb, K. *et al*. (2002). A fast and elitist multiobjective genetic algorithm: NSGA-II. *IEEE Transactions on Evolutionary Computation*, **6**, 2, pp. 182–197.

Dhanalakshmi, S. *et al*. (2011). Application of modified NSGA-II algorithm to Combined Economic and Emission Dispatch problem. *International Journal of Electrical Power & Energy Systems*, **33**, 4, pp. 992–1002.

Erbatur, F. *et al*. (2000). Optimal design of planar and space structures with genetic algorithms. *Computers & Structures*, **75**, 2, pp. 209–224.

Farshchin, M., Camp, C. V and Maniat, M. (2016). Multi-class teaching–learning-based optimization for truss design with frequency constraints. *Engineering Structures*, **106**, pp. 355–369.

Goldberg, D. E. (1989). *Genetic Algorithms in Search, Optimization, and Machine Learning*. *Reading, MA: Addison-Wesley*. Reading, MA: Addison-Wesley.

Gomes, H. M. (2011). Truss optimization with dynamic constraints using a particle swarm algorithm. *Expert Systems with Applications*, **38**, 1, pp. 957–968.

Hao, P. *et al*. (2017). An efficient adaptive-loop method for non-probabilistic reliability-based design optimization. *Computer Methods in Applied Mechanics and Engineering*, **324**, pp. 689–711.

Ho-Huu, V. *et al*. (2016). An effective reliability-based improved constrained differential evolution for reliability-based design optimization of truss structures. *Advances in Engineering*

Software, **92**, pp. 48–56.

Honda, S., Igarashi, T. and Narita, Y. (2013). Multi-objective optimization of curvilinear fiber shapes for laminated composite plates by using NSGA-II. *Composites Part B: Engineering*, **45**, 1, pp. 1071–1078.

Jalalpour, M., Guest, J. K. and Igusa, T. (2013). Reliability-based topology optimization of trusses with stochastic stiffness. *Structural Safety*, **43**, pp. 41–49.

Jeong, S.-B. and Park, G.-J. (2017). Single loop single vector approach using the conjugate gradient in reliability based design optimization. *Structural and Multidisciplinary Optimization*, **55**, 4, pp. 1329–1344.

Kannan, S. *et al*. (2009). Application of NSGA-II Algorithm to Generation Expansion Planning. *IEEE Transactions on Power Systems*.

Kaveh, A. (2017). Multi-Objective Optimization of Truss Structures. In*Advances in Metaheuristic Algorithms for Optimal Design of Structures* (pp. 603–631). Cham: Springer International Publishing.

Kaveh, A. and Ilchi Ghazaan, M. (2015). Hybridized optimization algorithms for design of trusses with multiple natural frequency constraints. *Advances in Engineering Software*, **79**, pp. 137–147.

Kaveh, A. and Talatahari, S. (2009). Particle swarm optimizer, ant colony strategy and harmony search scheme hybridized for optimization of truss structures. *Computers & Structures*, **87**, 5–6, pp. 267–283.

Kelesoglu, O. (2007). Fuzzy multiobjective optimization of truss-structures using genetic algorithm. *Advances in Engineering Software*, **38**, 10, pp. 717–721.

Khatibinia, M. and Sadegh Naseralavi, S. (2014). Truss optimization on shape and sizing with frequency constraints based on orthogonal multi-gravitational search algorithm. *Journal of Sound and Vibration*, **333**, 24, pp. 6349–6369.

Lamberti, L. (2008). An efficient simulated annealing algorithm for design optimization of truss structures. *Computers & Structures*, **86**, 19, pp. 1936–1953.

Lee, J.-O., Yang, Y.-S. and Ruy, W.-S. (2002). A comparative study on reliability-index and target-performance-based probabilistic structural design optimization. *Computers & Structures*, **80**, 3–4, pp. 257–269.

Lee, K. S. and Geem, Z. W. (2004). A new structural optimization method based on the harmony search algorithm. *Computers & Structures*, **82**, 9–10, pp. 781–798.

Li, F. *et al*. (2013). A single-loop deterministic method for reliability-based design optimization. *Engineering Optimization*, **45**, 4, pp. 435–458.

Li, L. J. *et al*. (2007). A heuristic particle swarm optimizer for optimization of pin connected structures. *Computers & Structures*, **85**, 7–8, pp. 340–349.

Liang, J., Mourelatos, Z. P. and Nikolaidis, E. (2007). A Single-Loop Approach for System Reliability-Based Design Optimization. *Journal of Mechanical Design*, **129**, 12, pp. 1215–1224. Retrieved from http://dx.doi.org/10.1115/1.2779884.

Lim, J. and Lee, B. (2016). A semi-single-loop method using approximation of most probable point for reliability-based design optimization. *Structural and Multidisciplinary Optimization*, **53**, 4, pp. 745–757.

Liu, G. R. and Chen, S. C. (2001). Flaw detection in sandwich plates based on time-harmonic response using genetic algorithm. *Computer Methods in Applied Mechanics and Engineering*, **190**, 42, pp. 5505–5514.

Liu, G. R., Ma, H. J. and Wang, Y. C. (2005). Material characterization of composite laminates

using dynamic response and real parameter-coded microgenetic algorithm. *Engineering with Computers*, **20**, 4, pp. 295–308.

Luh, G.-C. and Chueh, C.-H. (2004). Multi-objective optimal design of truss structure with immune algorithm. *Computers & Structures*, **82**, 11–12, pp. 829–844.

Mansour, R. and Olsson, M. (2016). Response surface single loop reliability-based design optimization with higher-order reliability assessment. *Structural and Multidisciplinary Optimization*, **54**, 1, pp. 63–79.

Marler, R. T. and Arora, J. S. (2004). Survey of multi-objective optimization methods for engineering. *Structural and Multidisciplinary Optimization*, **26**, 6, pp. 369–395.

Martínez-Vargas, A. *et al*. (2016). Application of NSGA-II algorithm to the spectrum assignment problem in spectrum sharing networks. *Applied Soft Computing*, **39**, pp. 188–198.

Meng, Z. *et al*. (2015). A hybrid chaos control approach of the performance measure functions for reliability-based design optimization. *Computers & Structures*, **146**, pp. 32–43.

Meng, Z. *et al*. (2017). A new directional stability transformation method of chaos control for first order reliability analysis. *Structural and Multidisciplinary Optimization*, **55**, 2, pp. 601–612.

Meng, Z. and Zhou, H. (2018). New target performance approach for a super parametric convex model of non-probabilistic reliability-based design optimization. *Computer Methods in Applied Mechanics and Engineering*, **339**, pp. 644–662.

Pelletier, J. L. and Vel, S. S. (2006). Multi-objective optimization of fiber reinforced composite laminates for strength, stiffness and minimal mass. *Computers & Structures*, **84**, 29–30, pp. 2065–2080.

Perez, R. E. and Behdinan, K. (2007). Particle swarm approach for structural design optimization. *Computers & Structures*, **85**, 19–20, pp. 1579–1588.

Pholdee, N. and Bureerat, S. (2012). Performance enhancement of multiobjective evolutionary optimisers for truss design using an approximate gradient. *Computers & Structures*, **106**, pp. 115–124.

Pholdee, N. and Bureerat, S. (2013). Hybridisation of real-code population-based incremental learning and differential evolution for multiobjective design of trusses. *Information Sciences*, **223**, pp. 136–152.

Richardson, J. N. *et al*. (2012). Multiobjective topology optimization of truss structures with kinematic stability repair. *Structural and Multidisciplinary Optimization*, **46**, 4, pp. 513–532.

Shan, S. and Wang, G. G. (2008). Reliable design space and complete single-loop reliability-based design optimization. *Reliability Engineering and System Safety*, **93**, 8, pp. 1218–1230.

Shayanfar, M., Abbasnia, R. and Khodam, A. (2014). Development of a GA-based method for reliability-based optimization of structures with discrete and continuous design variables using OpenSees and Tcl. *Finite Elements in Analysis and Design*, **90**, pp. 61–73.

Sonmez, M. (2011). Artificial Bee Colony algorithm for optimization of truss structures. *Applied Soft Computing*, **11**, 2, pp. 2406–2418.

Soyel, H., Tekguc, U. and Demirel, H. (2011). Application of NSGA-II to feature selection for facial expression recognition. *Computers & Electrical Engineering*, **37**, 6, pp. 1232–1240.

Srinivas, N. and Deb, K. (1994). Muiltiobjective Optimization Using Nondominated Sorting in Genetic Algorithms. *Evol. Comput.*, **2**, 3, pp. 221–248.

Xu, Y. G., Liu, G. R. and Wu, Z. P. (2002). Damage Detection for Composite Plates Using Lamb Waves and Projection Genetic Algorithm. *AIAA Journal*, **40**, 9, pp. 1860–1866.

Zhang, L.-Z. (2016). A reliability-based optimization of membrane-type total heat exchangers under uncertain design parameters. *Energy*, **101**, pp. 390–401.

Zhang, Q. and Li, H. (2007). MOEA/D: A Multiobjective Evolutionary Algorithm Based on Decomposition. *IEEE Transactions on Evolutionary Computation*.

Zheng, H. *et al*. (2005). Minimizing vibration response of cylindrical shells through layout optimization of passive constrained layer damping treatments. *Journal of Sound and Vibration*, **279**, 3–5, pp. 739–756.

Zitzler, E., Laumanns, M. and Thiele, L. (2001). SPEA2: Improving the strength Pareto evolutionary algorithm. In*Eurogen* (Vol. 3242, pp. 95–100).